Tungsten-Chromium-Yttrium alloys as first wall armor material: yttrium concentration, oxygen content and transmutation elements

Felix Klein[a], Mark R. Gilbert[b], Andrey Litnovsky[a], Jesus Gonzalez-Julian[a], Sophie Weckauf[a], Tobias Wegener[a], Janina Schmitz[a,c], Christian Linsmeier[a], Martin Bram[a], Jan Willem Coenen[a]

[a] *Forschungszentrum Jülich GmbH, Institut für Energie- und Klimaforschung, 52425 Jülich, Germany*
[b] *CCFE, United Kingdom Atomic Energy Authority, Culham Science Centre, Abingdon, Oxfordshire*
[c] *Department of Applied Physics, Ghent University, 9000 Ghent, Belgium*

Abstract

Tungsten (W) is a prime candidate as first wall armor material of future fusion power plants as W withstands extreme particle, heat, and radiation loads without forming long-lived radioactive waste. The release of radioactive material from the reactor to the environment should be suppressed in case of an accident such as a loss of coolant (LOCA) with simultaneous air ingress into the vacuum vessel. W oxidizes and sublimates in case of a LOCA. Therefore, oxidation resistant tungsten, chromium, yttrium (W-Cr-Y) alloys are developed to provide intrinsic safety in case of such an accident.

In this paper, the optimization of the yttrium (Y) concentration is presented on bulk samples compacted by field assisted sintering technology (FAST). W with 11.4 weight (wt) % Cr and 0.6 wt % Y appears to be an optimum regarding the oxidation resistance. Further, first preparations for industrial upscaling, which may increase the impurity level, are addressed. The oxygen (O) content is varied systematically. It is shown that a good oxidation resistance requires a low O level.

The exposure of the material to fusion neutrons is another issue addressed on W-Cr-Y alloys. In a non-activated environment it is shown that 1 wt % rhenium (Re) dramatically changes the oxidation kinetics: at 1273 K the mass gain of W-Cr-Y-Re follows a cubic rate law while W-Cr-Y follows a linear rate law for two days. Further, the influence of the alloying elements on the neutron transport and transmutation of W is studied by simulating the exposure of spatially heterogeneous high-resolution models of the W-Cr-Y alloys to 14 MeV fusion neutrons.

Keywords: Tungsten alloys, Oxidation resistance, Yttrium, Impurities, Transmutation, Neutrons

1. Introduction

Main advantages of W as first wall armor material in fusion power plants are its resistance to heat and particle loads, the good thermal conductivity and the low tritium retention. Neutrons from the plasma activate the W during regular operation. After five years of irradiation by a neutron flux expected in a DEMOnstration power plant, W is predicted to generate a heat of $6.19 \times 10^{-2}\,\mathrm{kW\,kg^{-1}}$. After 100 years the heat generation is reduced to $1.13 \times 10^{-10}\,\mathrm{kW\,kg^{-1}}$ [1]. The fast decay of the radioactive isotopes is another advantage of W as plasma-facing material.

However, the heat generation is a problem in case of a loss-of-coolant accident (LOCA) in combination with air ingress into the vacuum vessel. Temperatures between 1200 K and 1450 K for several weeks are predicted due to the nuclear decay heat in such an accident. The radioactive W oxidizes. The oxide sublimates at a rate of $1.4 \times 10^{-4}\,\mathrm{mg\,cm^{-2}\,s^{-1}}$ at 1273 K in humid air [2]. As this material can be released to the environment, sublimation is a severe safety hazard. Therefore, oxidation resistant W alloys are developed [2–9].

Email address: fe.klein@fz-juelich.de (Felix Klein)

Elemental optimization of the oxidation resistance based on thin films deposited by magnetron sputtering resulted in the optimum composition of an alloy containing W, 11.4 weight (wt) % of Cr, and 0.6 wt % of Y (W-11.4Cr-0.6Y) [4]. Field-assisted sintering technology (FAST) allowed the production of bulk samples of several millimeters [7], a thickness as foreseen for the first wall armor in DEMO [10]. A similar erosion resistance to the plasma as compared to pure W is shown [8]. Further, the sublimation is suppressed by more than one order of magnitude as compared to pure W in humid air at 1273 K [2].

This paper verifies that the Y content of 0.6 wt %, as optimized for thin films, is also optimum for the oxidation resistance of bulk alloys. Further, the influence of impurities on the oxidation resistance is addressed. Impurities can be introduced during manufacturing. Oxygen (O), one of the elements which is difficult to avoid, is investigated. Additionally, neutron irradiation during operation of the power plant transmutes W to rhenium (Re), tantalum (Ta), osmium (Os), and hafnium (Hf) [1]. The influence of Re as the main transmutation product on the oxidation resistance is studied. In addition, it is studied how the alloying elements influence the neutron transport and transmutation of W by simulating the exposure of spatially heterogeneous high-resolution models of the W-Cr-Y alloys to 14 MeV fusion neutrons.

2. Experimental methods

The first step of the sample production is the mechanical alloying of elementary W, Cr, and Y powders using a planetary ball mill. The powder is alloyed in a tungsten carbide (WC) milling jar using WC milling balls. The planetary mill PM400 manufactured by Retsch is continously operated at 250 rotations per minute for 60 h. The mechanical alloying results in a single phase powder. More details on the employed mechanical alloying process are described in [11].

The single phase powder is consolidated by Field Assisted Sintering Technology (FAST). During sintering there is a pressure of 50 MPa and the sample is heated at 200 K min^{-1} to the maximum sintering temperature of 1740 K from where it is immediately cooled at a rate of 300 K min^{-1}. More details on sintering and reasons for the selected parameters are adressed in [7].

The characterization of the alloys is performed using multiple methods:

X-ray diffraction (XRD) is performed using the device D8 Discover manufactured by Bruker AXS GmbH to measure the lattice structure of the material.

Electron microscopy is performed using the Crossbeam 540 manufactured by Carl Zeiss. Cross sections are cut using a focussed ion beam. Imaging is performed using an electron beam and secondary electrons while elemental analysis is performed by energy-dispersive X-ray spectroscopy (EDX). EDX results and the weighted amount of powder before alloying match, thus there is no selective loss of certain alloying elements.

Thermogravimetric analysis (TGA) is performed using the device TAG 16/18 manufactured by Setaram. The weight change of the alloy due to oxidation is recorded in-situ at 1273 K.

Chemical analysis on nitrogen (N) and oxygen (O) is performed using the LECO device TCH600. Calibration is performed using reference materials provided by LECO. The N content of the samples analyzed is (0.008 ± 0.001) wt %, it is not varied in this work. The influence of the O content on oxidation is studied in section 3.2.

The density is measured using Archimedes principle. A relative density of 98 % is measured for all W-alloys presented in this work.

3. Influence of the elemental composition on the oxidation

3.1. Yttrium content

The elemental composition of ternary W-11.4Cr-0.6Y alloys was optimized based on thin films [4]. Another study on samples compacted by Hot Isostatic Pressing (HIP) recommends the composition of W-10Cr-1Y [6]. Here, it is investigated whether the optimization remains valid for bulk alloys consolidated by FAST. The Cr concentration is kept constant, so that the elemental composition is W-11.4Cr-xY where the Y content x is varied. Four compositions containing $x = (0.3, 0.6, 1.0, 1.5)$ wt % Y are investigated. Fig. 1 shows cross sections of the four samples. All samples have a primary (αW, Cr) phase and Y-containing particles at the grain boundaries. In the images in Fig. 1 the Y-containing particles can be identified by a darker color. EDX analysis shows an increased Y and an increased O content as compared to the primary (αW, Cr) phase. Analysis of the stoichiometric composition and the Cr, W content of the particles requires more advanced analysis methods such as atom probe tomography as the information volume of EDX is larger than the Y-containing particles. Work is in progress which will be published elsewhere. According to preliminary results there are $YCrO_3$ particles.

Based on the planimetric procedure [12] grain and particle size are determined by graphical analysis: the number of grains and $YCrO_3$ particles on an area of 9 µm^2 are counted. Further, the number of pixels attributed to the $YCrO_3$ particles are counted. The results are summarized in table 1.

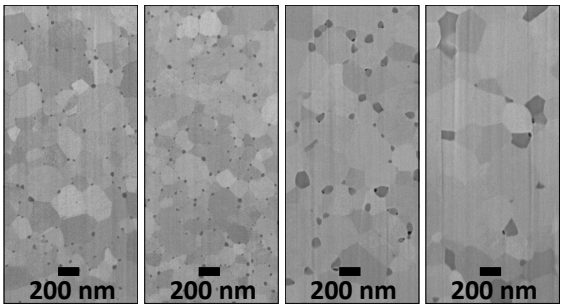

(a) 0.3 wt % Y (b) 0.6 wt % Y (c) 1.0 wt % Y (d) 1.5 wt % Y

Figure 1: Cross section images of four different W-11.4Cr-xY alloys. The Y content $x = (0.3, 0.6, 1.0, 1.5)$ wt % Y is given below each image. The same manufacturing parameters are used for each sample.

Table 1: Results of the graphical analysis of the cross sections shown in Fig. 1. n is the number of $YCrO_3$ particles on an area of 1 µm^2. d is the equivalent spherical diameter of the $YCrO_3$ particles. g is the equivalent spherical diameter of the grains in the primary (αW, Cr) phase.

wt % Y	0.3	0.6	1.0	1.5
n [µm^{-2}]	19	29	11	10
d [µm]	3×10^{-2}	3×10^{-2}	9×10^{-2}	15×10^{-2}
g [µm]	3.2×10^{-1}	2.5×10^{-1}	4.1×10^{-1}	4.2×10^{-1}

At $x = 0.3$ wt % Y the $YCrO_3$ particles are small and finely dispersed in the alloy, see Fig. 1 and table 1.

At $x = 0.6$ wt % Y the size of the $YCrO_3$ particles remains constant but the number of particles per unit area increases. The increased number of particles results in a more efficient reduction of grain growth during sintering. The grain size decreases as compared to the alloy containing 0.3 wt % Y, see Fig. 1 and table 1.

At $x = 1.0$ wt % Y the size of the $YCrO_3$ particles increases. An attractive force between the $YCrO_3$ particles causes a growth of the particles reducing the number of $YCrO_3$ particles per unit area as compared to the alloys with a lower Y content. This force appears only relevant once a sufficent density of $YCrO_3$ particles is present and the particles are in close vicinity of each other. The critical density appears to be above 29 µm^{-2} particles as measured for the W-11.4Cr-0.6Y alloy. The lower number of $YCrO_3$ particles allows stronger growth of the grains of the

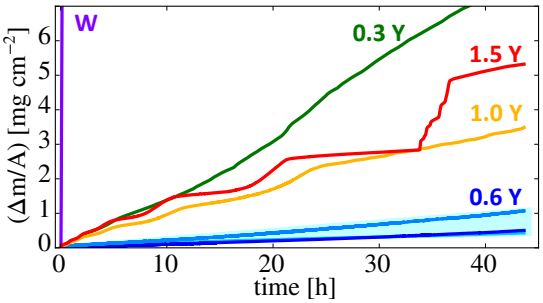

Figure 2: Mass change of W-11.4Cr-xY alloys and pure W as a function of time at a temperature of 1273 K in 20 kPa O_2 and 80 kPa Ar atmosphere. The yttrium content x is given in the labels.

primary (αW, Cr) phase during sintering as compared to the alloys with higher Y content, see Fig. 1 and table 1.

At $x = 1.5$ wt % Y the largest $YCrO_3$ particle size and the largest grain size of the investigated alloys is found, see table 1.

Oxidation experiments are performed at a temperature of 1273 K in 20 kPa O_2 and 80 kPa Ar atmosphere for 44 h. The results are shown in Fig. 2 and 3.

Fig. 2 shows the mass gain as a function of time. Lower mass gain corresponds to better oxidation resistance as less O reacts with the material. The best oxidation resistance is found for the W-11.4Cr-0.6Y alloys, which confirms the results based on thin films [4]. The measurement of the W-11.4Cr-0.6Y alloy is repeated three times for different samples produced via the same manufacturing route. An average linear oxidation rate of 4×10^{-6} mg cm^{-2} s^{-1} is measured, in all cases the oxidation rate is lower as compared the the oxidation rates of alloys with a different Y content.

As compared to the W-11.4Cr-0.6Y alloy, the average linear oxidation rate increased by a factor of 13, 6, and 8 for 0.3 wt % Y, 1.0 wt % Y, and 1.5 wt % Y, respectively. The linear oxidation rate of W is a factor of 1600 higher, as compared to W-11.4Cr-0.6Y. Further, the samples containing 0.3 wt % Y, 1.0 wt % Y, and 1.5 wt % Y exhibit breakaway oxidation.

X-ray diffractograms after oxidation at 1273 K are shown in Fig. 3. The main peaks of the W-11.4Cr-0.6Y alloy originate from the protective Cr_2O_3 and the metallic W alloy below the protective Cr_2O_3 layer. The other compositions have strong peaks corresponding to W-containing oxides, mainly present in the form of Cr_2WO_6. These oxides offer less protection and cause the higher mass gain shown in Fig. 2.

The study on samples compacted by HIP [6] confirms that 0.3 wt % Y is not sufficient for a good oxidation resistance. An optimum at 0.6 wt % Y is not excluded by their results as they tested at 0.5 wt % Y and 1.0 wt % Y finding that 1.0 wt % Y provides a better oxidation resistance. The lowest oxidation rate in [6] is a factor of 4 higher as compared to the best oxidation rate in this study. Also at 0.3 wt % Y the oxidation rate in [6] is a factor of 2 higher as the oxidation rate in this study at the same yttrium content. Reasons for the deviation in the oxidation rate are the different Cr content of 10 wt % Cr instead of 11.4 wt % Cr and the different microstructure as a result of the different compacting technology.

In conclusion, the fine adjustment to around 0.6 wt % Y is crucial for the formation of a protective Cr_2O_3 layer with a good diffusion barrier for incoming O and good adhesion to the alloy. At this Y concentration the highest density of $YCrO_3$ particles is achieved. These particles are crucial for the formation of small grains allowing diffusion of Cr towards the surface to form the protective oxide layer. Less Y results in less particles and worse oxidation resistance while more Y results in clustering to large particles which reduces the particle density and results in a worse oxidation resistance.

3.2. *Impurities introduced during manufacturing*

After optimization of the elemental composition presented in the previous section, preparations for industrial upscaling of oxidation resistant W alloys can start. Industrial upscaling creates the risk of an increase in impurities as compared to laboratory-samples, therefore it should be understood which impurities are to be avoided and which impurities can be tolerated. Elements which form long-lived radioactive isotopes must be avoided from neutron irradiation point of view. More information on waste implications from minor impurities is found in [17]. Degradation of the oxidation resistance due to impurities is another topic. Here, the influence of O on the oxidation resistance is studied. Previous studies always analyzed clean samples with 0.15 wt % O or less [2, 6, 11]. However, additional O can be introduced during alloying and sintering from the atmosphere.

Fig. 4 shows the mass gain as a function of time. The metallic composition is W-11.4Cr-0.6Y for all samples while the O content before oxidation is varied as given in the labels. The

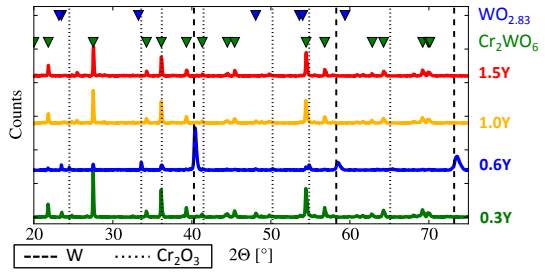

Figure 3: XRD measurements of W-11.4Cr-xY alloys after oxidation at 1273 K in 20 kPa O_2 and 80 kPa Ar atmosphere for 44 h. The Y content x is given in the labels. Peak positions for different compounds are marked. W, Cr_2O_3, Cr_2WO_6 and W_8O_{21} positions are based on [13–16], respectively.

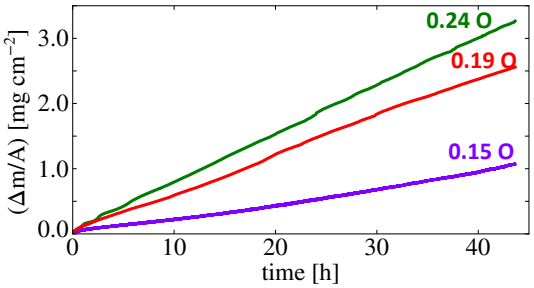

Figure 4: Mass change of W-11.4Cr-0.6Y alloys and pure W as a function of time at a temperature of 1273 K in 20 kPa O_2 and 80 kPa Ar atmosphere. The O content before oxidation in wt % is given in the labels.

Table 2: Linear oxidation rates k_l as a function of the O content before oxidation based on the data shown in Fig. 4.

wt % O	0.15	0.19	0.24
k_l [mg cm^{-2} s^{-1}]	6.5×10^{-6}	1.6×10^{-5}	2.0×10^{-5}

linear oxidation rates k_l for the three samples are given in table 2. The lowest mass gain is found for the alloy with the lowest O content before oxidation.

The presented results allow a hypothesis on the mechanism why O degrades the oxidation resistance, which is explained in the following. The solubility of O in W is very low - around 1 ppm is reported at room temperature for O on interstitial sites of W [18]. Thus, O impurities that have not reacted with Y must be located mainly in vacancies and at the grain boundaries. Cr diffuses mainly along the grain boundaries towards the surface. The more sites are occupied by O, the higher is the activation energy for the diffusion process of Cr. Consequently, the Cr flux to the surface is lower. A lack of Cr at the interface of the protective Cr_2O_3 and the metal causes W oxidation as observed in [5]. Oxidation of W causes a volumetric expansion and degradation of the protective oxide layer and should be avoided.

Y binds the O impurities in nano-particles (as seen in Fig. 1) where the O no longer hinders the Cr diffusion towards the surface. However, the capacity of the Y is limited. Theoretically, the reaction $2\,Y + 2\,Cr + 3\,O_2 \longrightarrow 2\,YCrO_3$ with 0.6 wt % Y can bind 0.32 wt % O.

The measurements show that 0.15 wt % O allows to form a protective Cr_2O_3 layer, as shown in Fig. 5. Interal oxidation of Cr is detected, but oxidation of W is successfully suppressed. In the case of a higher O content than 0.15 wt % O oxidation of W is observed. Thus, it is important to avoid O contamination during manufacturing and to keep the O content at 0.15 wt % or lower.

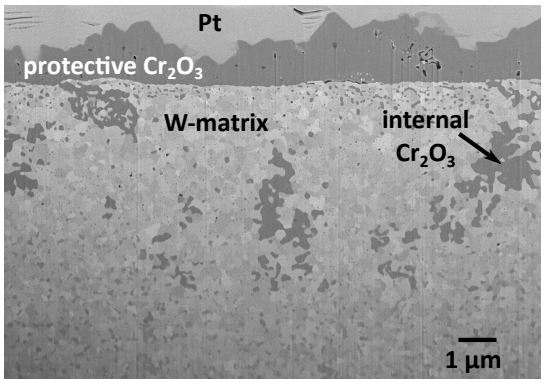

Figure 5: Cross section of the W-11.4Cr-0.6Y-0.15O alloy after oxidation at 1273 K for 44 h.

3.3. Impurities introduced during plasma operation

Neutron irradiation causes transmutations of the materials of the vacuum vessel. The transmutations cannot be avoided and it must be understood whether the transmutations influence the oxidation resistance. For example, pure W as first wall armor material after 2 years of DEMO operation is expected to contain 1 wt % Re, 0.2 wt % Ta, 0.08 wt % Os, and 0.001 wt % Hf [1].

Experimentally, the impact of the fusion neutron environment is studied using ion bombardment or by lower-energy neutron irradiations (typically in fission devices). However, the likely damage mechanisms are not well explored by these approaches because the ions are a proxy that, in particular, do not capture the correct time and length scales of fusion neutrons, while the energies and fluxes available in fission devices and other neutron experiments are not comparable to those predicted for DEMO.

Here, the influence of the main transmutation product, Re, on oxidation is studied in a non-activated environment by alloying Re into the material. A W-11.4Cr-0.6Y-1.0Re alloy is manufactured via the production route as described in section 2. W forms a solid solution with Re starting from 500 K for up to 24 wt % Re [19]. Thus, the authors assumed that Re would not influence the Cr transport significantly and would not have any significant influence on the oxidation resistance.

The oxidation resistance of the W-11.4Cr-0.6Y-1.0Re and the W-11.4Cr-0.6Y alloy is compared in Fig. 6 by measuring the mass change as a function of time at 1273 K. Fig. 6 a shows the mass gain while Fig. 6 b shows the gradient of the mass gain. W-Cr-Y shows a mass gain proportional to time (t). W-Cr-Y-Re exhibits a 3 times higher mass gain after the experiment time of 44 h. However, the mass change is proportional to $t^{1/3}$. The fit in Fig. 6 follows the function

$$\left(\frac{\Delta m}{A}\right)^3 = t \times 1.7 \times 10^{-4}\ \mathrm{mg^3\,cm^{-6}\,s^{-1}} \qquad (1)$$

where Δm is the mass change, A the surface area and t the time. This behavior yields faster oxidation during the first 20 h of the experiment while the gradient drops below the rate of W-Cr-Y after 40 h.

A linear oxidation rate indicates that the protective function of the oxide remains constant with increasing thickness of the oxide. Open channels through parts of the oxide remain available for O penetration. A parabolic oxidation rate indicates that there are no open channels and that the oxide growth is purely controlled by diffusion of Cr and O ions through the protective oxide layer. The cubic oxidation rate observed at the W-Cr-Y-Re alloy indicates a diffusion-controlled growth of the oxide combined with a mechanism to reduce the diffusion rate for longer oxidation times. For example [20] identified grain coarsening as such a mechanism. This mechanisms in the case of smart alloys is subject of future research.

The XRD (see Fig. 7) shows differences between W-Cr-Y and W-Cr-Y-Re after oxidation. The diffractogram of the oxidized W-Cr-Y alloy is dominated by peaks of the metallic alloy and Cr_2O_3. The diffractogram of the oxidized W-Cr-Y-Re alloy is dominated by peaks of Cr_2WO_6, peaks assigned to Cr_2O_3 are also detected while peaks of the metallic alloy are absent as the oxide on the surface is too thick to allow penetration of the X-rays.

The cross section of the W-11.4Cr-0.6Y-1.0Re alloy after sintering, before oxidation is shown in Fig. 8 a. The grain size increased to several micrometers as compared to a few hundred

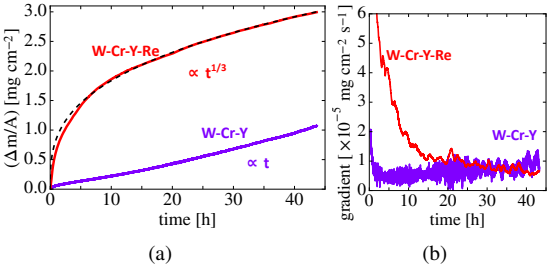

(a) (b)

Figure 6: (**a**) Mass change of a W-11.4Cr-0.6Y and a W-11.4Cr-0.6Y-1.0Re alloy as a function of time (t) at a temperature of 1273 K in 20 kPa O_2 and 80 kPa Ar atmosphere. (**b**) Gradient of the mass change measurements shown in (a).

nanometers in the ternary W-11.4Cr-0.6Y alloy. Further, a Cr-rich phase and large yttria particles are observed as shown in the EDX maps in Fig. 8 a. Re appears to be dissolved mainly in W. Future studies should investigate the reason for such a strong change in the microstructure as compared to the ternary W-11.4Cr-0.6Y alloy.

After oxidation there is an oxide layer with a thickness of 6.3 µm on the surface as shown in Fig.8 b. The Cr content decreases from the surface towards the interface of the oxide and the alloy. Only few W-rich particles are detected on the surface. The grain size of the alloy remains several micrometers, but a phase separation appears in some grains. Deeper understanding of the new phases requires a transmission electron microscopy study.

One question for future studies is the separate the effect of the change in microstructure and the effect of Re on the oxidation behavior as compared to that of W-11.4Cr-0.6Y. Thus, it should be attempted to manufacture a W-11.4Cr-0.6Y-1.0Re alloy with a microstructure similar to the ternary W-11.4Cr-0.6Y alloy. Another question is whether the cubic oxidation kinetics are maintained for longer times. In that case the oxidation resistance of W-Cr-Y-Re could be better as compared to that of W-Cr-Y. Longer studies should be conducted and be compared to the results published in [7]. Further, the potential release of radioactive material in case of a LOCA is determined by the sublimation rate. Thus, the sublimation rate must be measured to asses the performance of the alloy.

Generally, these results highlight the relevance to study the influence of neutron irradiation and transmutations on the oxidation resistance. The hypothesis that Re has a negligible influence on the oxidation resistance seems to be incorrect and more research in this field is required. The influence of the other transmutation products is another open question. An irradiation campaign would be the final step to understand the influence of irradiation on oxidation resistant W alloys.

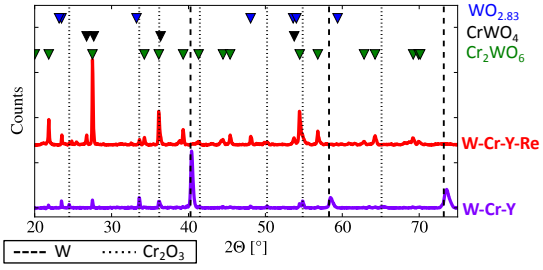

Figure 7: XRD after oxidation at a temperature of 1273 K in 20 kPa O_2 and 80 kPa Ar atmosphere for 44 h. The oxidation kinetics are shown in Fig. 6.

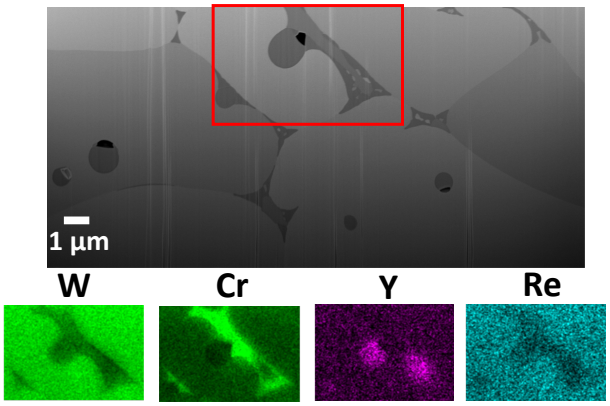

(a)

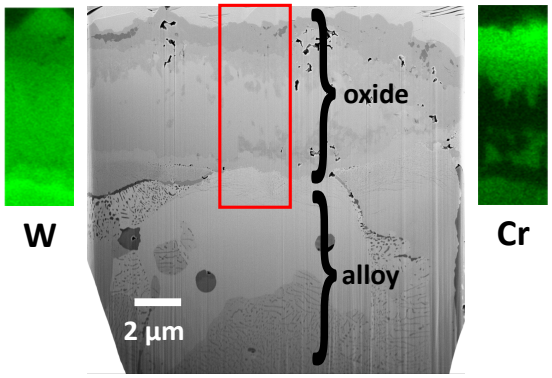

(b)

Figure 8: (**a**) Cross section of the W-11.4Cr-0.6Y-1.0Re alloy after sintering, including EDX maps at an acceleration voltage of 30 kV of W, Cr, Y, and Re in the marked region. (**b**) Cross section of the W-11.4Cr-0.6Y-1.0Re alloy after 44 h of oxidation at 1273 K including EDX maps at an acceleration voltage of 15 kV of W and Cr in the marked region.

4. Modeling neutron transport and transmutation

An irradiation campaign, as suggested in the previous section, is a complex experiment which should be prepared by modeling work. Therefore, this section presents first modeling results on neutron irradiation of smart alloys.

Extensive work is published on the transmutation rate of W under 14 MeV neutron irradiation [21]. High resolution models were developed to calculate the variation in transmutation on a scale of 0.1 mm. The local moderation of neutrons from surrounding water and steel at a 20 %-80 % by volume mix was considered. The calculations combined neutron transport simulations with MCNP [22] and inventory calculations with FISPACT-II [23]. The calculations are computationally expensive and use the following simplified geometry: in the center

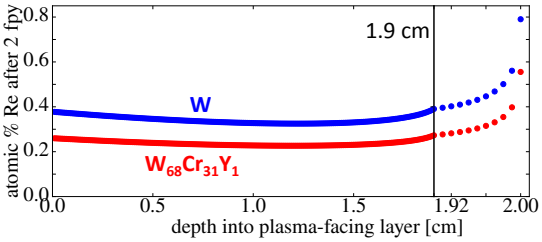

Figure 9: The transmutant Re concentration as a function of depth into the material after simulated 2 fpy of irradiation. Pure W and $W_{68}Cr_{31}Y_1$ are shown. The data for pure W is replicated from [21]. The final 1 mm is plotted on a higher resolution accounting for the large variation in Re concentration.

there is a fusion point source. It is surrounded by 2 cm spherical shell of W which is surrounded by a moderating shell of Fe and water. This geometry is scenario 1 in [21]. Full details on the computational methods are found in [21].

Here, the aim is to repeat the calculations presented in the aforementioned publication and substitute W by W-11.4Cr-0.6Y alloys to understand the influence of the alloying elements. In the following W-11.4Cr-0.6Y is given in atomic % as $W_{68}Cr_{31}Y_1$.

Fig. 9 shows the Re production due to transmutation as a function of depth after 2 full – power – years (fpy) of DEMO operation, which is expected to be roughly equivalent to a five-year lifetime of a first wall component (i.e. including downtime and maintenance periods). The Re production in the $W_{68}Cr_{31}Y_1$ alloy follows the same profile as pure W, but scaled according to the reduced W content. For both materials there is a strong increase in Re content to 0.8 at % at the back of the armor material near the steel/water moderator. More details on the mechanisms of the moderator are published in [21].

Similarly, a scaled profile according to the reduced W content is calculated for Os and Ta. Os is also influenced by moderation while the Ta production decreases with depth as shown for pure W in [21].

As compared to pure W, there are also the transmutation products of Cr. V is the main transmutation product from Cr. Fig. 10 shows that the V production is highest at the surface of the alloy at a low level of 0.05 at %. Other transmutation products of Cr are Ti, Mn, and Ca [1]. All these elements are contained in low concentrations, thus the studies on the influence on the oxidation resistance focused on the main transmutation product of the alloy, Re, see section 3.3.

Hydrogen (H) and helium (He) are other reaction products of

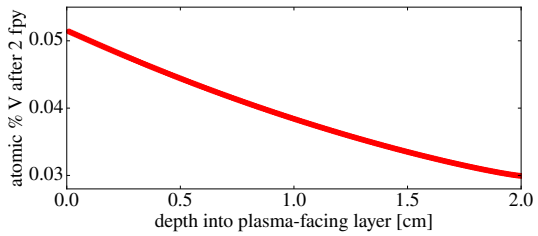

Figure 10: The transmutant V concentration as a function of depth into the $W_{68}Cr_{31}Y_1$ alloy after simulated 2 fpy of irradiation.

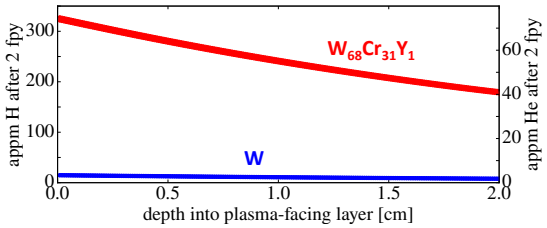

Figure 11: H and He gas production as a function of depth into the material after simulated 2 fpy of irradiation in atomic parts per million (appm). Pure W and $W_{68}Cr_{31}Y_1$ are compared.

the non-eleastic nuclear reaction between neutrons and the wall materials. The calculated gas production is shown in Fig. 11. The production of both, H and He, is increased by more than one order of magnitude in the $W_{68}Cr_{31}Y_1$ alloy as compared to pure W due to the presence of Cr. The nuclear reaction producing H and He requires fast neutrons, moderated neutrons cannot contribute [1]. Therefore, the gas production decreases almost linearly with depth as the fast neutrons decrease.

W exhibits fast H diffusion but an extremely low solubility limit [24]. Assuming a similar behavior in the W-Cr-Y alloy, H is not expected to accumulate in the material and can be gradually pumped out of the system.

Helium is reported to cause swelling and embrittlement of materials [25]. The solubility of He in the crystal lattice is low, thus He forms clusters and accumulates at grain boundaries and defects. This accumulation can cause a loss of structural integrity and limit the lifetimes of a material. The critical amount of He in the material is correlated to the grain size: the smaller the grain size the more grain boundaries are present the more He can be stored in the material without damaging the structural integrity. For a grain diameter of 0.5 µm the critical He concentration in W was estimated to be 9×10^2 atomic parts per million (appm) [26] which is more than one order of magnitude higher than the calculated He production, see Fig. 11. Considering that the grain size of the $W_{68}Cr_{31}Y_1$ alloy is only 0.3 µm the He production is not expected to cause problems.

5. Summary

W-11.4Cr-0.6Y alloys are a promising candidate as first wall armor material for future fusion power plants to provide intrinsic safety after a loss-of-coolant accident with simultaneous air ingress. Experiments presented in this paper show that 0.6 wt % is the optimum Y concentration providing a large number of Y-containing nano-particles while avoiding the clustering to larger particles.

Further it is shown that a low level of O impurities is important for the oxidation resistance of the alloy. The Y should react with most of the O so that the O does not hinder the formation of a protective Cr_2O_3 layer.

Issues related to the exposure to 14 MeV neutrons are addressed. The main transmutation product of W under 14 MeV neutron irradiation is Re. Adding Re by alloying in a non-activated environment dramatically changes the oxidation kinetics from a linear to a cubic rate law at 1273 K. Further studies on

the reasons for the cubic oxidation kinetics, sublimation studies, and longer oxidation experiments should be conducted. The experimental work is complemented by modeling work. Simulations of the exposure of spatially heterogeneous high-resolution models suggest that the production of W transmutants scales down with the W concentration. The presence of Cr causes increased production of V, H, and He. All production rates are estimated to be at a non-critical rate.

Acknowledgements

A part of this work has been carried out within the framework of the EUROfusion Consortium and has received funding from the Euratom research and training programme 2014 - 2018 and 2019 - 2020 under grant agreement No 633053. The views and opinions expressed herein do not necessarily reflect those of the European Commission.

References

[1] M. R. Gilbert, J.-C. Sublet, and R. A. Forrest. *Handbook of activation, transmutation, and radiation damage properties of the elements simulated using FISPACT-II & TENDL*. Culham Center For Fusion Energy, 2015.

[2] F. Klein, A. Litnovsky, T. Wegener, X. Y. Tan, J. Gonzalez-Julian, M. Rasinski, J. Schmitz, Ch. Linsmeier, M. Bram, and J. W. Coenen. Sublimation of advanced tungsten alloys under DEMO relevant accidental conditions. *Fusion Eng. Des.*, 146(A):1198–1202, 2019.

[3] F. Koch, J. Brinkmann, S. Lindig, T. P. Mishra, and Ch. Linsmeier. Oxidation behaviour of silicon-free tungsten alloys for use as the first wall material. *Phys. Scr.*, 2011(T145):014019, 2011.

[4] T. Wegener, F. Klein, A. Litnovsky, M. Rasinski, J. Brinkmann, F. Koch, and Ch. Linsmeier. Development of yttrium-containing self-passivating tungsten alloys for future fusion power plants. *Nucl. Mater. Energy*, 9:394–398, 2016.

[5] F. Klein, T. Wegener, A. Litnovsky, M. Rasinski, X. Y. Tan, J. Schmitz, Ch. Linsmeier, J. W. Coenen, H. Du, J. Mayer, and U. Breuer. On oxidation resistance mechanisms at 1273 K of tungsten-based alloys containing chromium and yttria. *Metals*, 8(7):488, 2018.

[6] A. Calvo, K. Schlueter, E. Tejado, G. Pintsuk, N. Ordas, I. Iturriza, R. Neu, J. Y. Pastor, and C. Garcia-Rosales. Self-passivating tungsten alloys of the system W-Cr-Y for high temperature applications. *Int. J. Refract. Met. Hard Mater.*, 73:29–37, 2018.

[7] F. Klein, T. Wegener, A. Litnovsky, M. Rasinski, X. Y. Tan, J. Gonzalez-Julian, J. Schmitz, M. Bram, J. W. Coenen, and Ch. Linsmeier. Oxidation resistance of bulk plasma-facing tungsten alloys. *Nucl. Mater. Energy*, 15:226–231, 2018.

[8] J. Schmitz, A. Litnovsky, F. Klein, X. Y. Tan, U. Breuer, M. Rasinski, S. Ertmer, A. Kreter, J. Gonzalez-Julian, M. Bram, et al. Argon-seeded plasma exposure and oxidation performance of tungsten-chromium-yttrium smart alloys. *Tungsten*, 2661-8036:1–10, 2019.

[9] J. Schmitz, A. Litnovsky, F. Klein, T. Wegener, X. Y. Tan, M. Rasinski, A. Mutzke, P. Hansen, A. Kreter, A. Pospieszczyk, et al. WCrY smart alloys as advanced plasma-facing materials - exposure to steady-state pure deuterium plasmas in PSI-2. *Nucl. Mater. Energy*, 15:220–225, 2018.

[10] Yu. Igitkhanov, B. Bazylev, I. Landman, and R. Fetzer. Design strategy for the PFC in DEMO reactor. *KIT Scientific Publishing*, KIT-SR 7637, 2013.

[11] A. Litnovsky, T. Wegener, F. Klein, Ch. Linsmeier, M. Rasinski, A. Kreter, X.Y. Tan, J. Schmitz, J. W. Coenen, Y. Mao, et al. New oxidation-resistant tungsten alloys for use in the nuclear fusion reactors. *Phys. Scr.*, 2017(T170):014012, 2017.

[12] ASTM Committee E-4 on Metallography, editor. *ASTM E112-13, Standard Test Methods for Determining Average Grain Size*. ASTM International, West Conshohocken, PA, United States, 1996.

[13] H. E. Swanson. *Standard X-ray Diffraction Powder Patterns*, volume 1, p. 28. Natl. Bur. Stand. (U. S.), 1953.

[14] H. F. McMurdie, M. C. Morris, E. H. Evans, B. Paretzkin, W. Wong-Ng, L. Ettlinger, and C. R. Hubbard. Standard x-ray diffraction powder patterns from the JCPDS research associateship. *Powder Diffr.*, 1(2):64–77, 1986.

[15] W. Kunnmann, S. La Placa, L.M. Corliss, J. M. Hastings, and E. Banks. Magnetic structures of the ordered trirutiles Cr_2WO_6, Cr_2TeO_6 and Fe_2TeO_6. *J. Phys. Chem. Solids*, 29(8):1359–1364, 1968.

[16] Yu. A. Barabanenkov, N. D. Zakharov, I. P. Zibrov, V. P. Filonenko, P. Werner, A. I. Popov, and M. D. Valkovskii. High-pressure phases in the system W-O. II. structure determination of $WO_{2.625}$ by HRTEM and x-ray powder diffraction analysis. *Acta Cryst.*, B49(2):165, 1993.

[17] M. R. Gilbert, T. Eade, T. Rey, R. Vale, C. Bachmann, U. Fischer, and N. P. Taylor. Waste implications from minor impurities in european DEMO materials. *Nucl. Fusion*, 59(7):076015, 2019.

[18] E. Lassner and W. D. Schubert. *Tungsten: Properties, Chemistry, Technology of the Element, Alloys, and Chemical Compounds*. Springer Science+Business Media, LLC, 1999.

[19] Z.-K. Liu and Y. A. Chang. Evaluation of the thermodynamic properties of the Re-Ta and Re-W systems. *J. Alloys Compd.*, 299(1-2):153–162, 2000.

[20] D. J. Tallman, B. Anasori, and M. W. Barsoum. A critical review of the oxidation of Ti_2AlC, Ti_3AlC_2 and Cr_2AlC in air. *Mater. Res. Lett.*, 1(3):115–125, 2013.

[21] M. R. Gilbert, J.-Ch. Sublet, and S. L. Dudarev. Spatial heterogeneity of tungsten transmutation in a fusion device. *Nucl. Fusion*, 57(044002), 2017.

[22] Mcnp6 user manual, version 1.0 2013 edited by d. b. pelowitz, los alamos document number: La-cp-13-00634, rev. 0. further details at http://mcnp.lanl.gov/.

[23] J.-Ch. Sublet, J. W. Eastwood, J. G. Morgan, M. R. Gilbert, M. Fleming, and W. Arter. FISPACT-II: An advanced simulation system for activation, transmutation and material modelling. *Nuclear Data Sheets*, 139, 2017.

[24] Jo. Roth and K. Schmid. Hydrogen in tungsten as plasma-facing material. *Phys. Scr.*, 2011(T145):014031, 2011.

[25] T. Yamamoto, G. R. Odette, H. Kishimoto, J. W. Rensman, and P. Miao. On the effects of irradiation and helium on the yieldstress changes and hardening and non-hardeningembrittlement of $\sim$ 8 Cr tempered martensitic steels: Compilation and analysis of existing data. *J. Nucl. Mater.*, 356(1-3):27–49, 2006.

[26] M. R. Gilbert, S. L. Dudarev, S. Zheng, L. W. Packer, and J.-Ch. Sublet. An integrated model for materials in a fusion power plant: transmutation, gas production, and helium embrittlement under neutron irradiation. *Nucl. Fusion*, 52(8):083019, 2012.